Development of a Systematic Methodology for Active Noise Control With Vehicle Engine Mounts Excitation

Kyoung-Jin Chang

Sound Design Research Lab, Hyundai Motor Company, Hwaseong 18280, Republic of Korea. E-mail: changkj@hyundai.com

Simon Roberts

ISVR Consulting, University of Southampton, Southampton SO17 1BJ, United Kingdom.

(Received 3 August 2023; accepted 9 October 2023)

Active noise control (ANC) technology using speakers as actuators has an excellent performance, but since it generates anti-noise signals in a path completely different from the vehicle's noise source, performance can be greatly reduced at a location far from the error sensor, and this problem can get worse as the frequency to be controlled increases. Another approach is the vibration-based ANC technology that excites the body member around the engine mount and reduces acoustic error signals in a passenger compartment. This approach has the advantage of being effective even at a distance from the error sensor and reducing vibration and noise together when trying to cancel out the structure borne noise generated by the engine because the paths from the primary source and the secondary source to the interior are almost identical. This paper presents a systematic methodology for this vibration-based ANC technology to achieve high performance in vehicles. First, through noise reduction simulation, the number of error sensors, the location of actuators, the force requirements, and an appropriate system are proposed. Next, to improve performance even with a small number of actuators and limited power when applying this technology in vehicles, an algorithm using the control effort weighting parameter is introduced into the existing FxLMS algorithm and modelled on the controller. Finally, a noise reduction control test is performed in a vehicle under static and driving conditions, and the results are reviewed.

NOMENCLATURE

p	number of reference microphones
q	number of actuators, i.e. secondary sources
r	number of error microphones
$\boldsymbol{p}_d$	disturbance pressure vector at reference points
$\boldsymbol{p}_r$	residual pressure vector at reference points
$\boldsymbol{p}_e$	measured pressure vector at error microphones
$\boldsymbol{f}$	estimated force vector of actuators
$\boldsymbol{H}_n$	noise transfer function matrix $(p \times q)$ at reference points
$\boldsymbol{H}_e$	noise transfer function matrix $(r \times q)$ at error microphones
n	sample time number
L	length of the FIR filter representing the secondary path plant
α	convergence coefficient
α_g	frequency independent convergence coefficient
α_f	frequency dependent convergence coefficient
ω_c	frequency of disturbance signal, i.e. control frequency
λ_m	m-th eigenvalue
δ	regularisation factor
β	control effort weighting parameter
p	limit voltage
u	demand voltage
$\boldsymbol{w}(n)$	$(2q \times 1)$ control filter coefficient vector at the n-th sample time
$w_{\boldsymbol{qI}}, w_{\boldsymbol{qQ}}$	in-phase and quadrature filter coefficients at the q-th secondary source, respectively
$r_{\boldsymbol{rqI}}$, $r_{\boldsymbol{rqQ}}$	in-phase and quadrature reference signals filtered by the plant response from the r-th error sensor to the q-th secondary source, respectively.
$\boldsymbol{s_{rq}}$	plant response filter from the r-th error sensor to the q-th secondary source
$\boldsymbol{x_I}(n), \boldsymbol{x_Q}(n)$	in-phase and quadrature reference signal vector over the past L samples
$\boldsymbol{e}(n)$	$r\times 1)$ error signal vector at the nth sample time
$\boldsymbol{d}(n)$	$(r \times 1)$ disturbance signal vector at the n-th sample time
$\boldsymbol{R}(n)$	$(r \times 2q)$ filtered reference signal matrix
$\widehat{\boldsymbol{R}}(n)$	$(r \times 2q)$ estimated filtered-reference signal matrix
$\widehat{\boldsymbol{S}}(j\omega)$	$r \times 2q)$ estimated secondary path plant response matrix at frequency ω
ANC	active noise control
FxLMS	filtered-x least mean square
WOT	wide open throttle
NTFs	noise transfer functions

1. INTRODUCTION

Active noise control (ANC) technology has been studied over decades and has made a lot of progress.[1] This technology can be a very effective tool for tonal noise at low frequencies, so it is widely used to reduce vehicle noise.[2,3] In general, most conventional ANC technologies that reduce noise use audio speakers, but there are also several basic studies on how to cancel out noise using vibration generation.[4–8] Fuller introduced an active structural acoustic control (ASAC) system that reduces noise by considering the sound radiation efficiency of structural modal vibration in low frequency bands using piezoelectric ceramic actuators mounted on a panel.[4] Oliveira conducted a study to improve psychoacoustic metrics in the passenger compartment using a structural sensor/actuator pair while exciting engine noise in the vehicle mockup.[5] Shoreshi and Buttelmann conducted an active vibro-acoustic control study to reduce engine noise using a feed forward algorithm and an active absorber mounted on a frame in a real vehicle.[6,7] Kraus conducted an active control study to reduce engine noise by installing active engine mounts based on piezo actuators in a real vehicle.[8]

Overall, approaches to reduce noise caused by the engine of vehicles through active noise control can be classified as follows. The first approach is a conventional ANC method that uses audio speakers of a vehicle, which has the advantage of not requiring an actuator of a secondary path in addition to the existing audio system.[2,3] However, since anti-noise signals are generated in a path completely different from the noise source, control performance may be greatly reduced at a location far from the error sensor and control stability may be degraded under certain conditions of the vehicle.

The second approach is the ANC method using the body-mounted vibration actuator proposed in K.-J. Chang's study, where vibration actuators are attached to body panels near a passenger compartment that are effective for sound radiation, such as cowl top panels, and error microphones are set up in the vehicle to apply the Filtered-x Least Mean Square (FxLMS) algorithm.[9] This method has the advantage of being able to control structure borne noise with a small number of vibration actuators. However, since the secondary path is long and different from the primary path, various supplementary algorithms are necessary to improve control stability in vehicles.

The third approach to be introduced in this paper is a modified form of the second approach, in which vibration actuators are attached to the body member around engine mounts corresponding to the noise transmission path, and error microphones for FxLMS are set up in the vehicle. This method is effective in reducing structure borne noise, such as the noise caused by engine vibration, and has the disadvantage of requiring a number of actuators because vibration actuators must be added for each noise transmission path. However, since the primary path and the secondary path are almost identical, this method has the advantage of being stable, being naturally effective at a location far from the error sensor and reducing not only noise but also vibration. Based on the third approach, this study proposes to build a methodology for the development of an ANC system that reduces engine noise through vibration actuators attached to engine mounts while driving.

In this study, first the noise to be controlled is identified, and the excitation position that is most effective in reducing engine noise is selected through static simulation of noise control. In addition, the excitation force required for noise reduction is estimated to propose the actuator suitable for the ANC of a target vehicle. Next, algorithms with hardware constraints are added to the FxLMS algorithm to increase performance when this method is implemented in vehicles. Finally, ANC tests are performed while actually driving the vehicle.

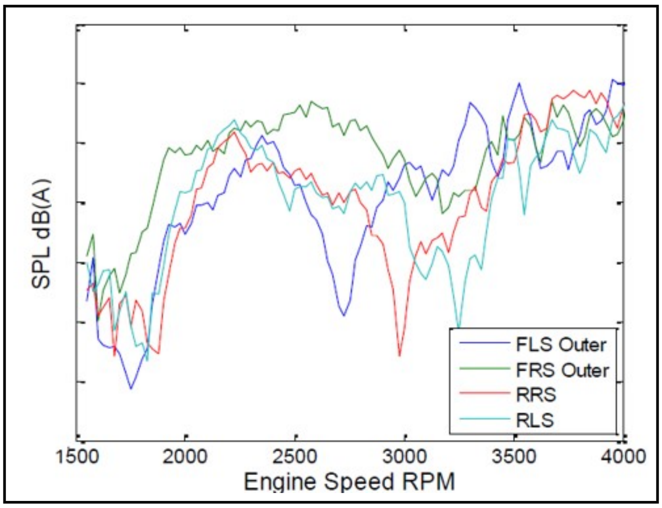

Figure 1. The second order noise measurements of a diesel car.

2. PRE-TEST AND SIMULATION

2.1. Base Measurement and Target Selection

In order to identify the noise to be controlled in this study, a test has been conducted to measure the baseline noise of the vehicle prior to noise control. Noise is measured on a diesel vehicle, accelerating up to 4000 rpm under 3rd gear under wide open throttle (WOT) conditions. A total of four microphones are installed at the driver's outer ear position, the passenger's outer ear position, the center of the rear left seat, and the center of the rear right seat for noise measurement. Figure 1 shows the noise levels at four points by extracting the second order component, the most dominant component of the four-cylinder engine, from the measured noise. This second order noise accounts for the most of booming noise inside a vehicle. From the results, significant booming noise can be seen between 1800 rpm and 3000 rpm corresponding to 60–100 Hz band, and the noise reduction with ANC is the primary issue of this study.

2.2. Positioning of Error Sensors and Actuators

Some of the seven reference microphones installed in the passenger compartment will be selected as error sensors, and some of the nine points of the front body member close to the engine mounts which are the structural transmission paths of engine noise will be selected as actuator positions for ANC as shown in Figure 2. Figure 3 shows the noise transfer functions (NTFs) between the driver's outer ear and the nine actuator positions measured in a vehicle, where one scale interval of the noise level is 10 dB. The frequency band requiring noise control is 40 to 150 Hz, which corresponds to 1200 to 4500 rpm of the second order engine noise. The best location of error sensors and actuators is determined through the following static simulation of noise control, where the noise reduction effect in the steady state is estimated from the vehicle's FRF and

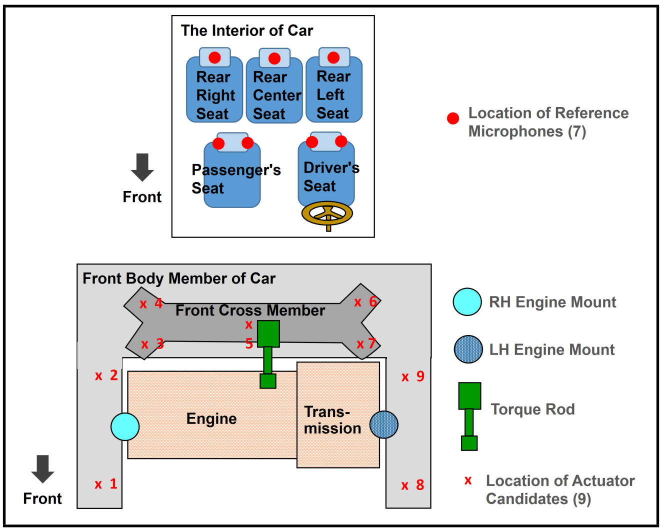

Figure 2. Location of reference microphones and actuator candidates in a vehicle.

noise measurements. This static simulation is repeated to find the most appropriate location and the minimum number of actuators required for ANC. These calculations are based on a steady state minimization of the sound pressure level at the interior, reference microphones, given by Eqs. (1) and (2).

$$\boldsymbol{p}_r = \boldsymbol{p}_d - \boldsymbol{H}_n \boldsymbol{f}; \tag{1}$$

$$\boldsymbol{f} = \boldsymbol{H}_e^{-1} \boldsymbol{p}_e. \tag{2}$$

For this calculation, the error sensors are the four microphones measured earlier and are a subset of the reference microphones. From this simulation, two points of the left and right-side members of the front body, i.e. points 2 and 8, have been selected as the most effective excitation positions for noise reduction. Figures 4 and 5 are simulation results that statically predict the noise reduction effect using Eqs. (1) and (2). Figure 4 is the result predicted when the actuators operate individually at the two points selected above, and Figure 5 is the result predicted when the actuators operate at these two points at once. As illustrated in Figure 4, a significant reduction in the second order engine noise levels is shown at a low speed, but a reduction at 3000 rpm or higher is limited. However, Figure 5 shows a sufficient noise reduction even at high rpm by increasing the level of force required when operating both actuators at the same time. Therefore, if maximum control performance is guaranteed, noise reduction effects of about 15 dB or more are expected at 1800–3000 rpm and about 10 dB above 3000 rpm.

2.3. Excitation Force Estimation and Actuator Selection

The actuator force required to achieve the desired noise reduction can be estimated from Eq. (2). As a result, the force requirement for using only one actuator is shown in Figure 6, and the force requirement for using two actuators is shown in Figure 7. Since each actuator operates effectively at 1800–3000 rpm, which is the primary band of interest, the force required when using two actuators is less than when using one. Using these results, Physics IV40, an electromagnetic inertial actuator as shown in Figure 8, has been proposed for ANC testing of the vehicle. This actuator is slightly lacking in power in the high frequency band, but it has a very large resonance in the low frequency band of approximately 40 Hz and can generate a force of approximately 20 N to 30 N at 40 Hz to 150 Hz. However, since the maximum force required in the target frequency band of Figure 7 is about 50 N, the actuator is expected to generate insufficient force to obtain the desired noise control effect. Nevertheless, the reason this actuator has been selected is because it is the product that can generate the greatest force within the size and weight that can be attached around the engine mount of the vehicle. In order to efficiently distribute power to actuators and avoid overrun issues, this study introduces a beta scheduling algorithm that efficiently distributes driving voltage and limits power, which will be described in the next chapter. Figure 9 shows the results of predicting the noise reduction effect with two actuators attached to points 2 and 8 under steady state conditions. In comparing these results with Figure 5, it is shown that the effect is slightly insufficient above 3000 rpm due to the limited force of the actuator, but there is still significant noise reduction at 1800–3000 rpm.

2.4. Comparison with the Case of Exciting Body Panels

In order to compare the case of exciting on the body member around engine mounts with the case of exciting on the body panel near the passenger compartment, which was introduced in the previous study, the noise reduction effect is also estimated when an actuator is attached to the cowl top panel. It is assumed that the actuator is mounted at point 15 corresponding to the center of the cowl top panel as shown in Figure 10. Figure 11 is the simulation result of potentially estimating the noise reduction effect in the steady state by the method described in the previous section, and the result shows a slightly insufficient but almost similar noise reduction effect compared to the case with the engine mounts shown in Figure 5. Figure 12 shows the prediction of the force required for noise control, which seems to require less than 10 N in the entire frequency band. When comparing these results with Figure 7, the force required to excite the body panel is much smaller than that of the engine mounts, indicating that the ANC method of exciting the body panel is advantageous in terms of miniaturization of the actuator. However, as introduced in in K.-J. Chang's research, there is a problem with the long impulse response function of the secondary path due to the excitation of the vehicle body panel degrading control stability.[9] So this study will focus on the ANC method that excites around the engine mounts.

2.5. Reducing Error Sensors

In order to compare the noise reduction effect according to the number of error sensors, noise reduction has been predicted when only two of the four error sensors are used in the driver's seat and the passenger's seat. Figure 13 shows the results of predicting the reduction of the second order engine noise using the offline model of the ANC algorithm to be introduced in the next chapter. The results show that the noise control effect of using four error sensors is slightly more advantageous overall than that of using two error sensors. However, even when using two error sensors, it has been found that there is still a large noise reduction effect not only in the front seat but also in the rear seat. As mentioned in the introduction, that is

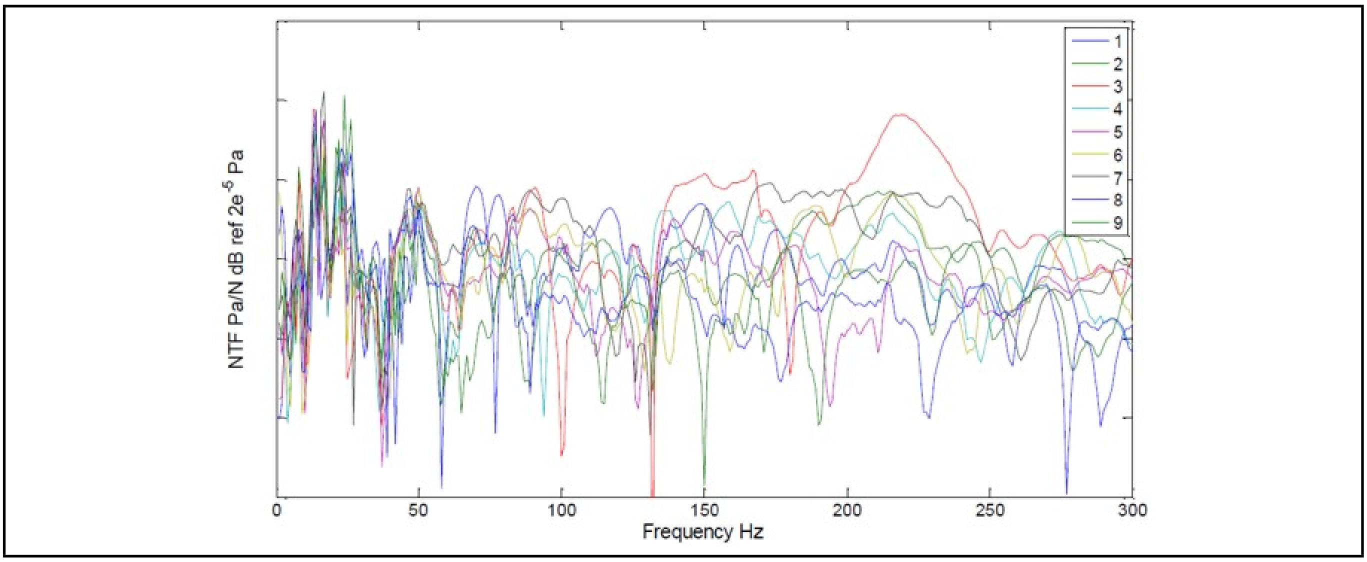

Figure 3. Measured NTFs between the driver's outer ear and the nine actuator positions.

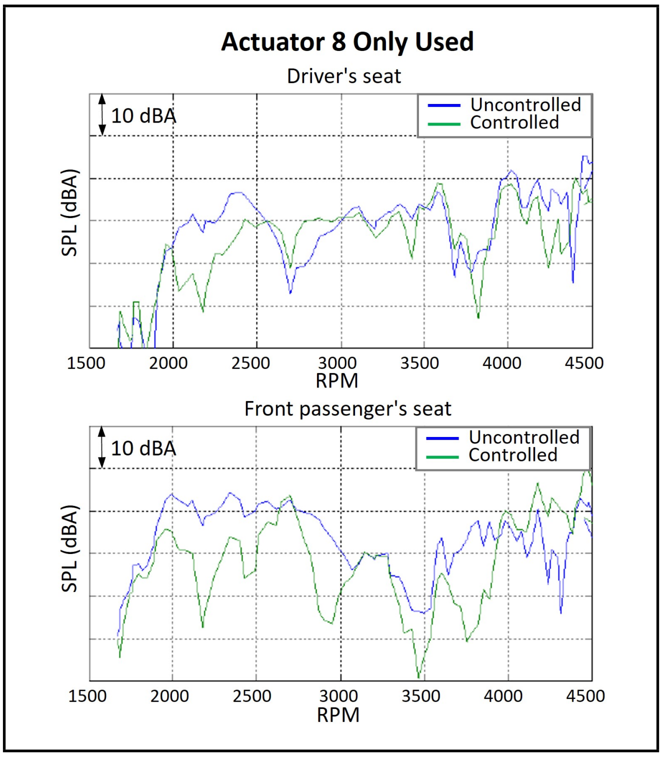

Figure 4. Simulation results of steady state noise reductions with single actuators.

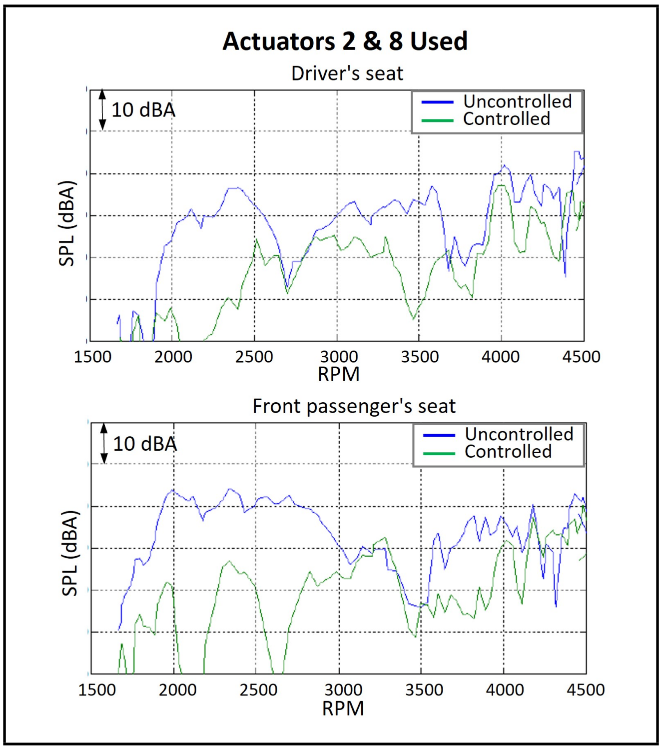

Figure 5. Simulation results of steady state noise reductions with two actuators.

an advantage of this method to excite the engine mount, because this method has the effect of controlling structure borne noise even at positions away from the error sensor, e.g. the rear center seat shown in Figure 2. Therefore, if cost reduction is necessary, it is possible to reduce the number of error sensors to less than two, and detailed research on this will be left as a follow-up study. In this study, four error sensors are maintained to improve the performance of all seats.

3. ANC ALGORITHM

3.1. Theoretical Background

The multichannel filtered-x LMS algorithm is widely known, and the behavior of the adaptive system can be completely described by a matrix of linear, time invariant, transfer functions.[10–13] It can be presented for the specific case of controlling a single frequency using r error sensors, q control sources, L coefficient control filters as shown in Figure 14. The error signal vector at the n-th sample is approximated by:

$$\boldsymbol{e}(n) = \boldsymbol{d}(n) + \boldsymbol{R}(n)\boldsymbol{w}(n). \tag{3}$$

In Eq. (3), the control filter coefficient vector, $\boldsymbol{w} = \left[\boldsymbol{w}_1^T, \boldsymbol{w}_2^T, \ldots, \boldsymbol{w}_q^T\right]^T$ where the filter coefficient vector of the q-th source can be divided into the in-phase and quadrature components such as $\boldsymbol{w_q} = [w_q I, w_q Q]^T$. Also, the filtered

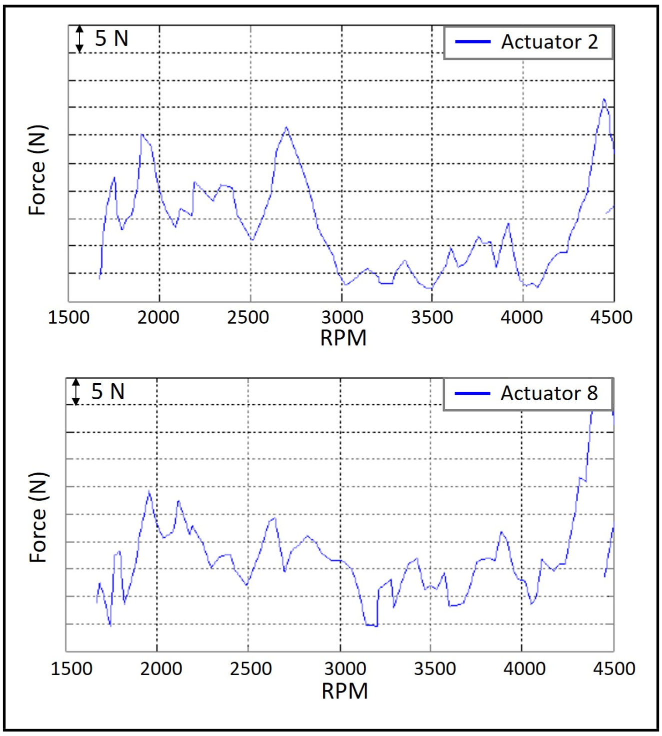

Figure 6. Actual force requirement with single actuators.

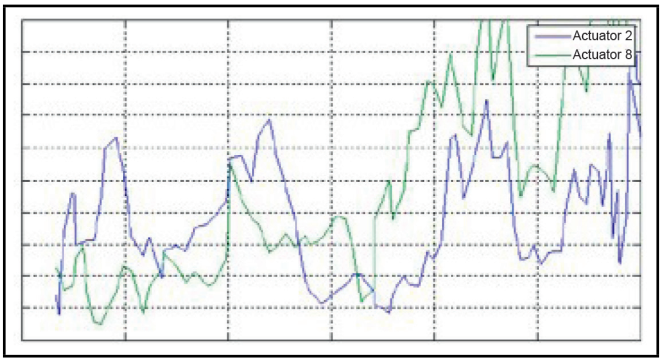

Figure 7. Actual force requirement with two actuators.

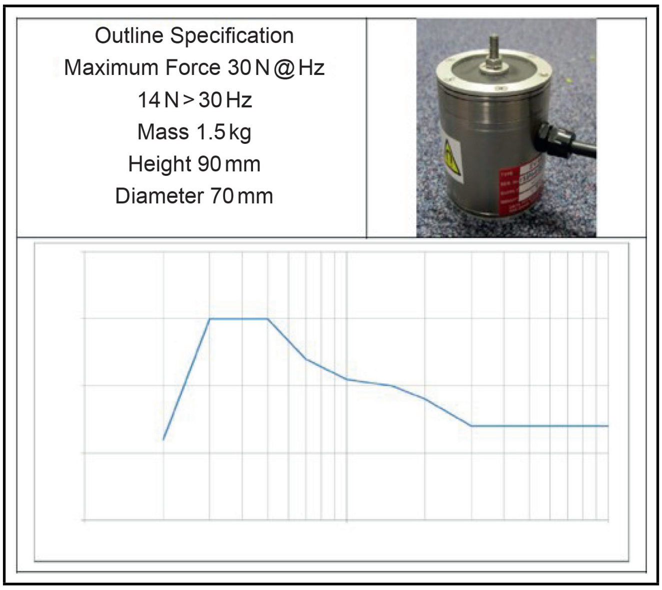

Figure 8. Specification of the inertial actuator used in the ANC test.

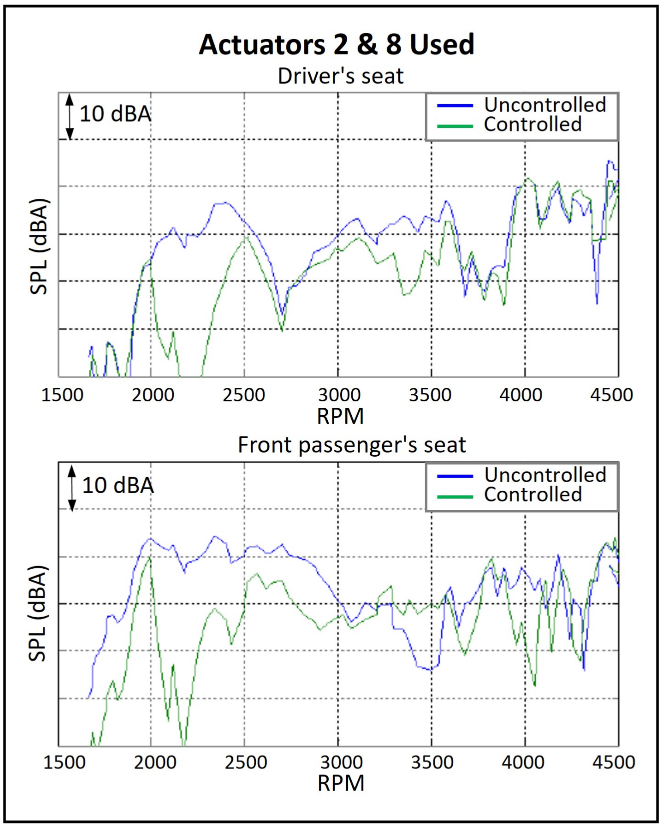

Figure 9. Predicted steady state noise reductions with two actuators attached to points 2 and 8 under steady state conditions.

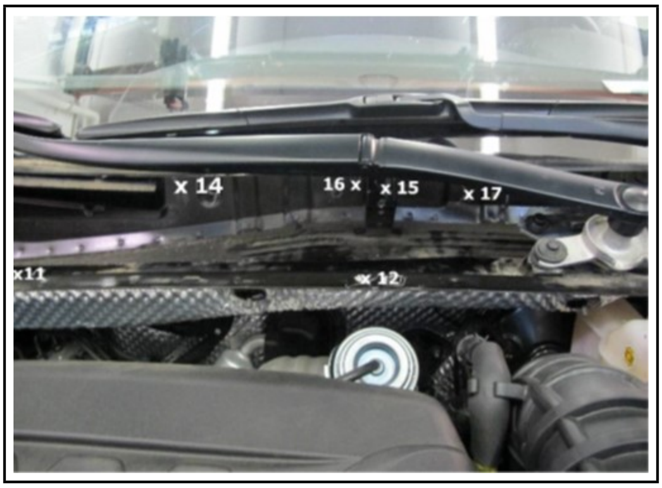

Figure 10. Location of the actuator for excitation on the cowl top panel.

reference signal matrix is $\boldsymbol{R}(n) = \begin{bmatrix} \boldsymbol{r}_1^T(n) \\ \boldsymbol{r}_2^T(n) \\ \vdots \\ \boldsymbol{r}_r^T(n) \end{bmatrix}$ where the filtered reference signal matrix of the r-th error sensor, $\boldsymbol{r_r} = [r_{r1I}, r_{r1Q}, \cdots, r_{rqI}, r_{rqQ}]^T$. In more detail, r_{rqI} is the in-phase reference signal filtered by the plant response from the r-th error sensor to the q-th secondary source as shown in:

$$\boldsymbol{r_r q I}(n) = \boldsymbol{s_{rq}} * \boldsymbol{x_I}(n); \tag{4}$$

where $\boldsymbol{s_{rq}}$ is the L coefficient FIR filter representing the plant response from the r-th error sensor to the q-th secondary source and $\boldsymbol{x_I}(n)$ is the in-phase reference sig-

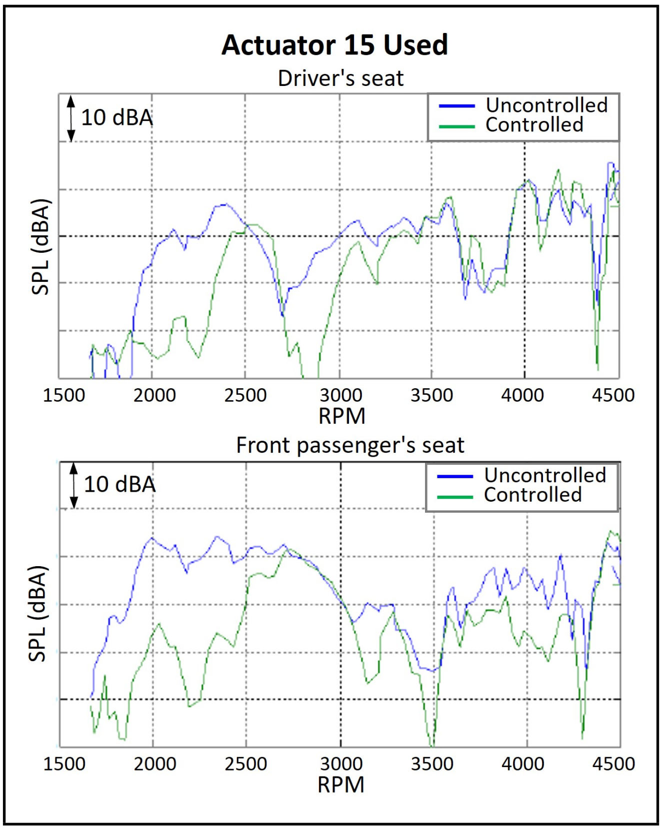

Figure 11. Simulation results of steady state noise reductions when one actuator is mounted on the cowl top panel.

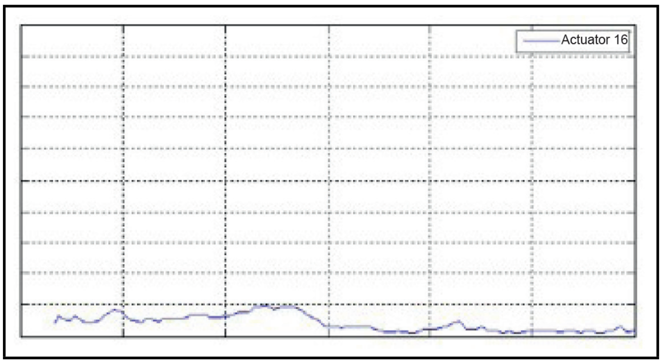

Figure 12. Actual force requirement when one actuator is mounted on the cowl top panel.

nal vector over the past L samples, i.e. $\boldsymbol{x_I}(n) = [x_I(n), x_I(n-1), \ldots, x_I(n-L+1)]^T$. In the same way, $\boldsymbol{r_{rqQ}}$ is the quadrature reference signal filtered by the plant response from the r-th error sensor to the q-th secondary source as shown in:

$$\boldsymbol{r_{rqQ}}(n) = \boldsymbol{s_{rq}} * \boldsymbol{x_Q}(n); \tag{5}$$

where $\boldsymbol{x_Q}(n)$ is the quadrature reference signal vector over the past L samples, i.e. $\boldsymbol{x_Q}(n) = [x_Q(n), x_Q(n-1), \ldots, x_Q(n-L+1)]^T$.

Minimizing the sum of the squared error signals and using the instantaneous gradient estimate, the filter update equation of FxLMS controller can be derived as:

$$\boldsymbol{w}(n+1) = \boldsymbol{w}(n) - \alpha \widehat{\boldsymbol{R}}^{\boldsymbol{T}}(n)\boldsymbol{e}(n); \tag{6}$$

where $\widehat{\boldsymbol{R}}(n)$ can be obtained by using the estimated model of the plant responses in the Eqs. (4) and (5). Also, the con-

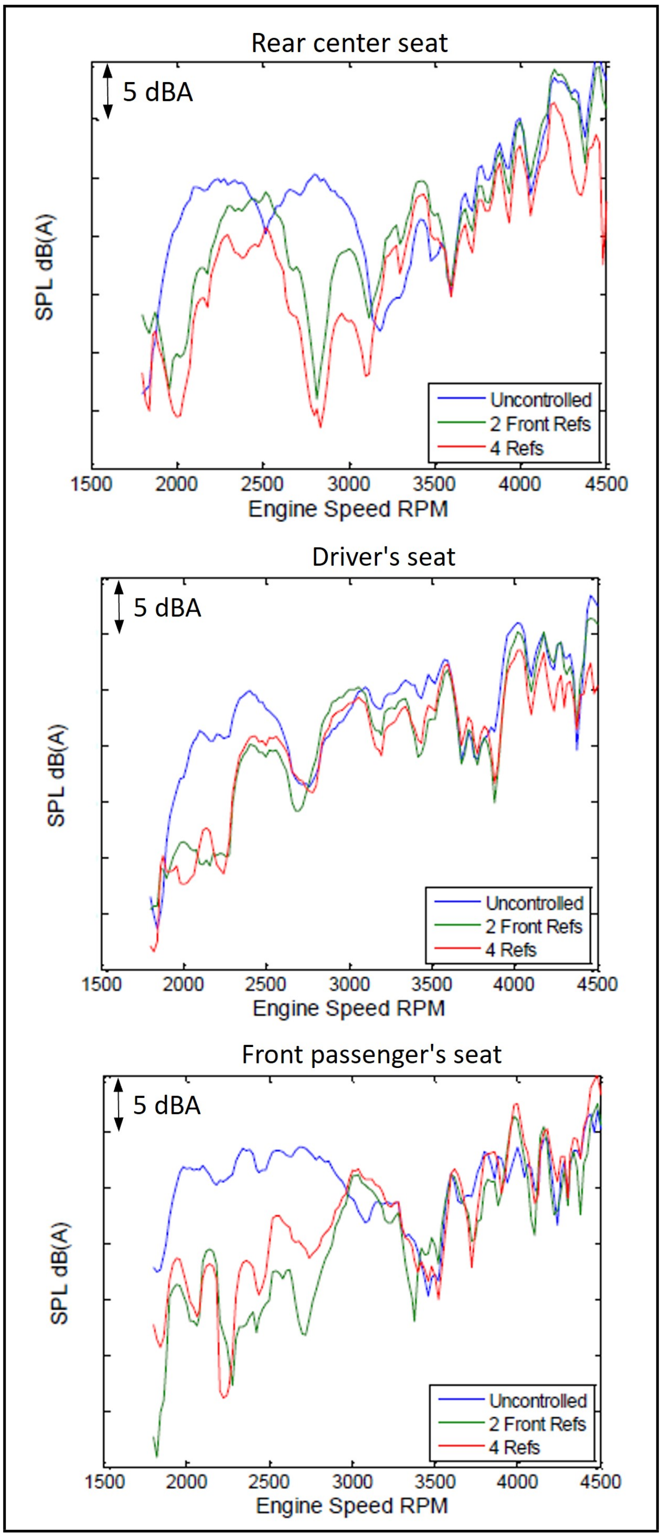

Figure 13. Predicted off-line ANC effects depending on the number of error sensors.

vergence condition of the multichannel FxLMS algorithm has been derived in other publications and for the general case of a stochastic disturbance signal is given by:

$$0 < \alpha < \frac{2Re(\lambda_m)}{|\lambda_m|^2} \quad \text{for all} \quad \lambda_m; \tag{7}$$

where λ_m are the complex eigenvalues of the matrix $E\left[\widehat{\boldsymbol{R}}^{\boldsymbol{T}}(n)\widehat{\boldsymbol{R}}(n)\right]$.[12] For a tonal controller where the reference signal is a pure tone like an engine noise, those can be replaced

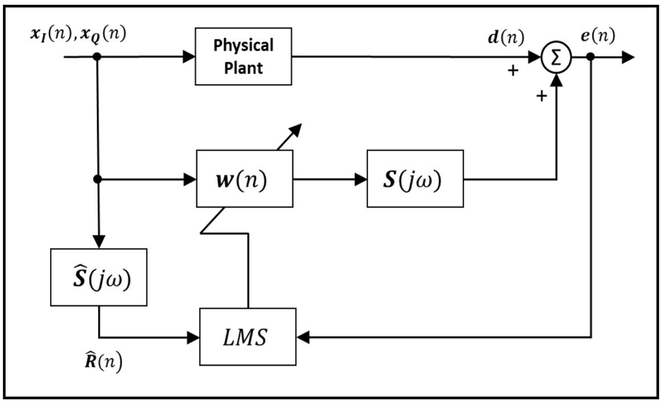

Figure 14. A block diagram of the multichannel narrowband FxLMS algorithm.

by the eigenvalues of the matrix $E\left[\widehat{\boldsymbol{S}}^{\boldsymbol{H}}(j\omega_c)\ \widehat{\boldsymbol{S}}(j\omega_c)\right]$. From Eq. (7), the constant value of alpha can be selected to be stable in all frequency bands, but it is recommended to employ a frequency dependent convergence coefficient to improve the performance of the controller. The filter update equation of the normalized FxLMS algorithm can be written as:

$$\boldsymbol{w}(n+1) = \boldsymbol{w}(n) - \alpha(n)\widehat{\boldsymbol{R}}^{\boldsymbol{T}}(n)\boldsymbol{e}(n); \qquad (8)$$

where the convergence coefficient can be composed of the two terms as shown in:

$$\alpha(n) = \alpha_g \alpha_f(\omega_c); \qquad (9)$$

where α_g is the frequency independent convergence coefficient that can be obtained by trade-off between convergence and accuracy and $\alpha_f(\omega_c)$ is the frequency dependent convergence coefficient that can be scheduled on the frequency of the disturbance signal. Simply, $\alpha_f(\omega_c)$ncan be obtained according to the maximum bound given by Eq. (7) using the largest eigenvalue of $E\left[\widehat{\boldsymbol{S}}^{\boldsymbol{H}}(j\omega_c)\ \widehat{\boldsymbol{S}}(j\omega_c)\right]$.[13]

In addition, various normalization procedures have been introduced to improve the control stability and performance.[14,15] One of them is given by:

$$\alpha_f(\omega_c) = E\left[\widehat{\boldsymbol{S}}^{\boldsymbol{H}}(j\omega_c)\,\widehat{\boldsymbol{S}}(j\omega_c) + \delta\boldsymbol{I}\right]^{-1}; \qquad (10)$$

where δ is a regularisation factor which can be used to improve the robustness of the algorithm.

However, in actual control cases, it is necessary not only to minimize the cost function of the error signal, but also to impose constraints on the electrical power required by the control system. In this study, the beta scheduling method has been adopted as follows to show the efficient performance of the controller and avoid the overrun issue.[13] For a tonal controller, in the time domain the cost function with a constraint on the control effort can be expressed as:

$$J_{cost}(n) = \boldsymbol{e}^T(n)\boldsymbol{e}(n) + \beta\boldsymbol{w}^T(n)\boldsymbol{w}(n); \qquad (11)$$

where β is the control effort weighting parameter. This cost function includes the instantaneous sum of the squared error signals and a term proportional to the sum of the squared control signals. The derivative of Eq. (11) with respect to the filter coefficients can be given as:

$$\frac{\partial J_{cost}(n)}{\partial \boldsymbol{w}(n)} = 2\left[\widehat{\boldsymbol{R}}^{\boldsymbol{T}}(n)\boldsymbol{e}(n) + \beta\boldsymbol{w}(n)\right]. \qquad (12)$$

Therefore, the filter update equation can be derived as:

$$\boldsymbol{w}(n+1) = (1-\alpha(n)\beta)\,\boldsymbol{w}(n) - \alpha\widehat{\boldsymbol{R}}^{\boldsymbol{T}}(n)\boldsymbol{e}(n); \qquad (13)$$

where, β acts as a total control effort constraint while the individual control effort constraints for imposing power limits on individual actuators can be derived from the reference.[13] A simple expression of β in voltage is as follows:

$$\beta = \left|\frac{1}{(p^2-u^2)} - \frac{1}{p^2}\right|; \qquad (14)$$

where p is the limit voltage and u is the demand voltage.

3.2. Coding and Porting to Controller

The normalized multichannel FxLMS algorithm with beta scheduler introduced in the previous section has been coded in the Mathworks Simulink and ported to the Microautobox II. The cosine function and sine function created according to the engine rpm received through the vehicle's CAN information are used as the reference signals, $\boldsymbol{x_I}(n)$ and $\boldsymbol{x_Q}(n)$, and the sampling frequency is set at 2048 Hz. Figure 15 illustrates the schematic of the overall model built by Simulink. Figure 16 is the Controller block among detailed blocks, where the two principal blocks represent the FxLMS controller with the in-phase and quadrature control blocks. The additional blocks calculate the frequency dependent parameters of the controller. These include the convergence coefficient α, the control effort weighting parameter β and a frequency dependent output limiter to prevent over driving of the actuators. In the block "Beta_Scheduler", individually for each actuator, the appropriate value of β is determined between the maximum allowable driving voltage and the instantaneous required voltage, where the maximum allowable driving voltage is programmed in advance in a frequency-based lookup table as shown in the block "PI vs Freq" in Figure 16. Prior to the block, "Beta_Scheduler" the maximum allowable voltage is squared and then multiplied by a constant which can be tuned during development. There are two branches to the β calculation subroutine depending on the magnitude of the demand, and this is handled by a conditional block. The value of β is set to 1 if the demand is greater than or equal to the pre-set limit value. If the demand is below the limit value, β is calculated according to the Eq. (14).

Figure 17 shows the maximum value of the frequency dependent convergence coefficient α for vehicle ANC control, which was obtained from Eq. (9). This value can be modelled as a lookup table, and this study uses 95% of the maximum value shown. Figure 18 shows the relationship between demand voltage and the control effort weighting parameter β deciding the power leakage and control effect, where the β levels of the squared voltage and linear voltage are compared. The use of the squared voltage rather than the linear voltage allows a greater rate of progression to be achieved and delays the application of leakage at lower drive voltages. During operation, β is kept as low as possible to maximize system response, but the value increases as the demand for actuators increases.

Figure 21 shows the structure of FxLMS controller: the structures of the in-phase and quadrature controllers are identical. The plant model is implemented by multiple FIR filter blocks which are applied to the supplied reference signal. This is done in parallel for all the actuators and the responses

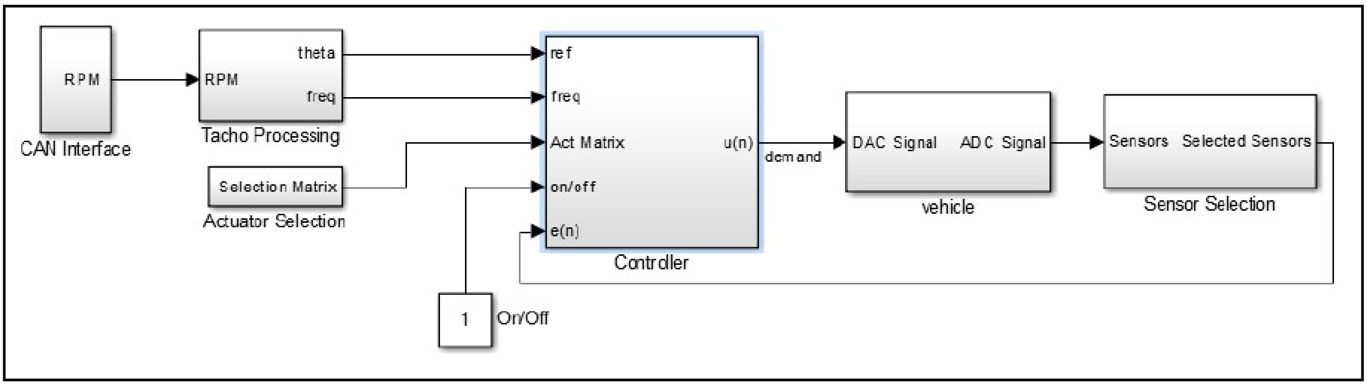

Figure 15. Schematic of overall model.

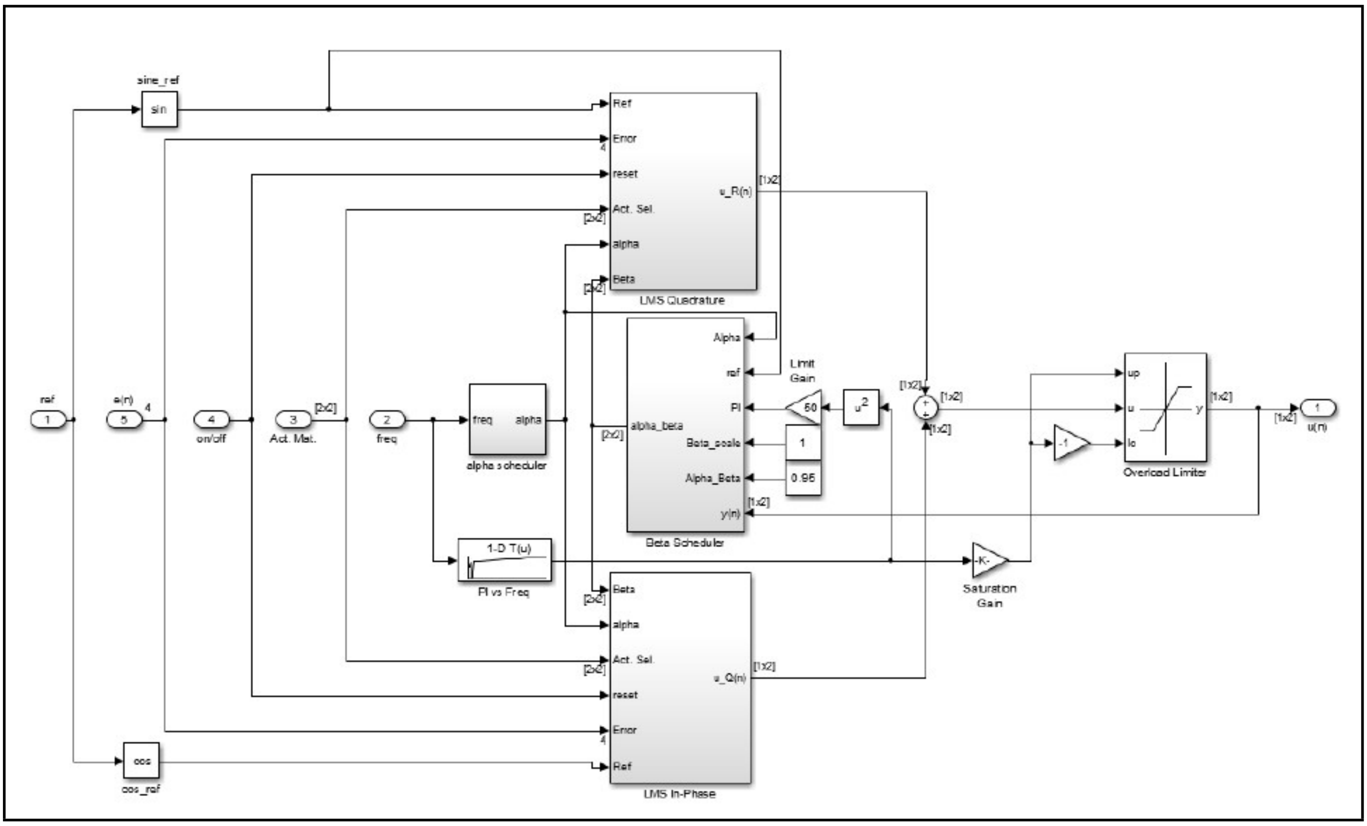

Figure 16. Schematic of the Controller block.

are combined into a matrix which is then transposed to allow multiplication with the current error estimate. Prior to this, the error estimate is scaled by the current value of the convergence coefficient α supplied through input 5. The block "Actuator Selection" multiplies the filtered error vector by a diagonal matrix of weightings for the individual actuators, allowing some to be turned off as required. The output of the block, "Beta_Scheduler" is introduced through input port 6 and applied to the filter weightings in the feedback loop. The controller can be turned off by forcing the filter coefficients to zero which is done by the block, "reset switch". The FxLMS controller uses FIR filters to represent the secondary path plant response, and the system identification routine required to measure the FIR filter coefficients is run prior to compilation of the main control program. Figure 22 shows the schematic of the system identification process. The excitation is applied using a logarithmic swept sine. The actuator used can be selected interactively and the filter taps are captured by the dSpace system to a Matlab file. Due to the non-linear amplitude characteristics of the actuators a lookup table is used to change the amplitude depending on the frequency of the excitation.

4. ANC TEST

4.1. Static Steady State Test

This section describes the ANC test process of a test vehicle in real time. Three test conditions are considered: (1) Static steady-state test at 2000 rpm no load; (2) Static run up test in no load; and (3) Driving test at a 3rd gear WOT. Since the above two conditions, i.e. (1) and (2), do not include disturbances such as road noise, there is an advantage that it may be controlled by focusing more on engine noise. As described in Sections 2.2 to 2.3, two actuators are installed vertically on the left and right points of the front body side members, and a total of seven microphones are set up in the vehicle, including four error microphones on the front left, front right, rear left, and rear right. Figure 19 shows a picture of the actuators, microphones and a control system installed in a vehicle. ANC test

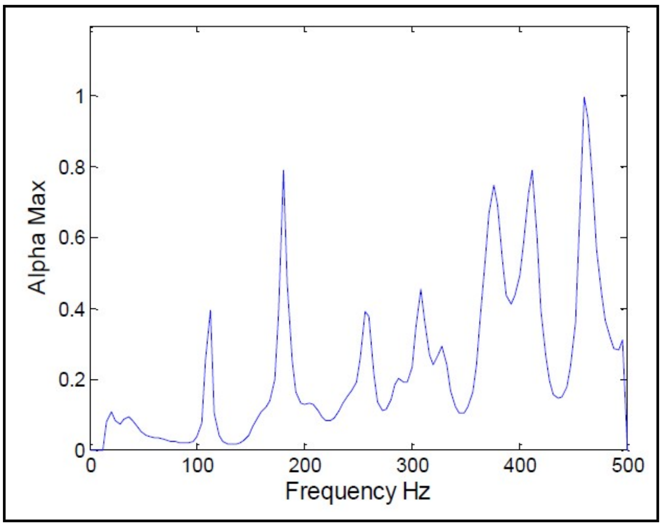

Figure 17. Frequency dependent convergence coefficient.

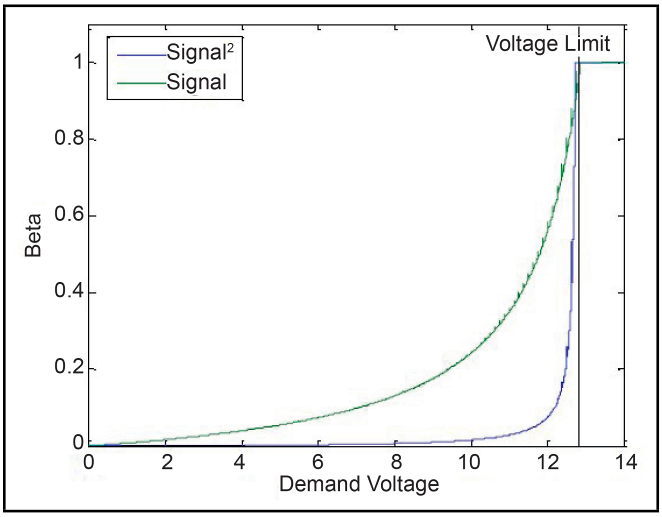

Figure 18. Relationship between a demand voltage and a control effort weighting parameter.

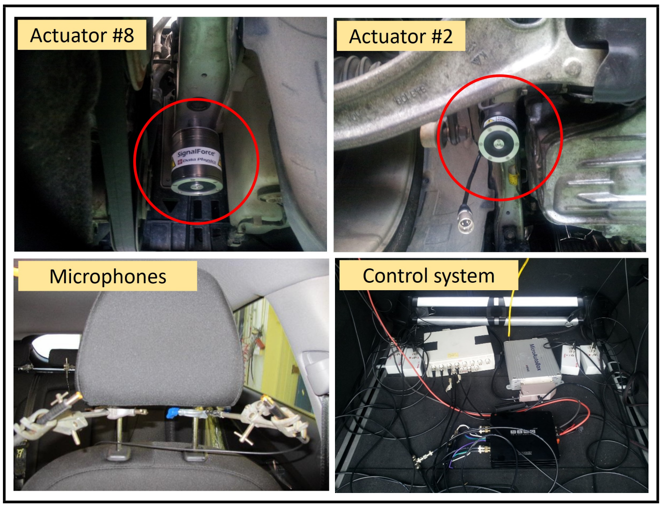

Figure 19. Picture of the actuators, microphones and a control system installed in a vehicle.

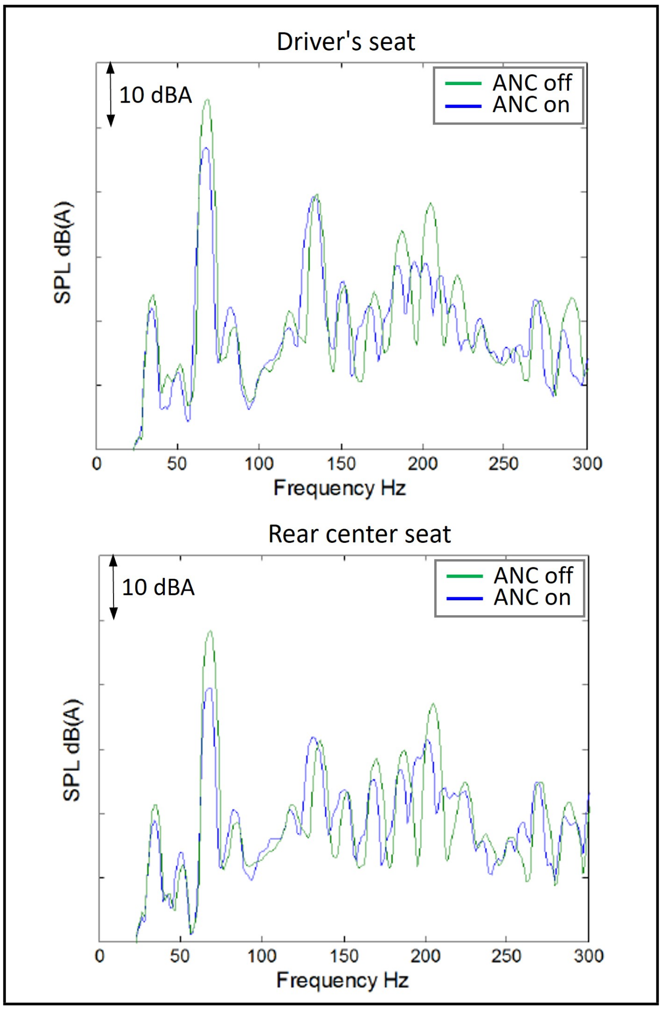

Figure 20. ANC test results at 2000 rpm no-load.

results for a static steady-state, measured at 2000 rpm with no load at the driver's seat and the rear center seat, are shown in Figure 20. These indicate that a reduction of between 8 dB and 10 dB is achieved at the frequency band of primary issue, i.e. 60–100 Hz.

4.2. Static Run-up Test

ANC test results for a static run-up are shown in Figure 23 which includes the responses at the two front microphones and the rear center microphone. The engine speed against time is also displayed, and the results indicate the run-up rate is fairly slow, taking approximately 15 s to rise 1000 rpm. These results indicate a reduction of up to 8 dB with the main changes between 1800 rpm and 3000 rpm which is the primary noise issue.

4.3. Driving Test

The ANC test results for a 3rd gear WOT acceleration are shown in Figure 24. Again, this shows the results for the two front microphones and the rear center microphone with the engine rpm. These results indicate a reduction of up to 7 dB with the main changes between 1800 rpm and 3000 rpm which is the primary noise issue.

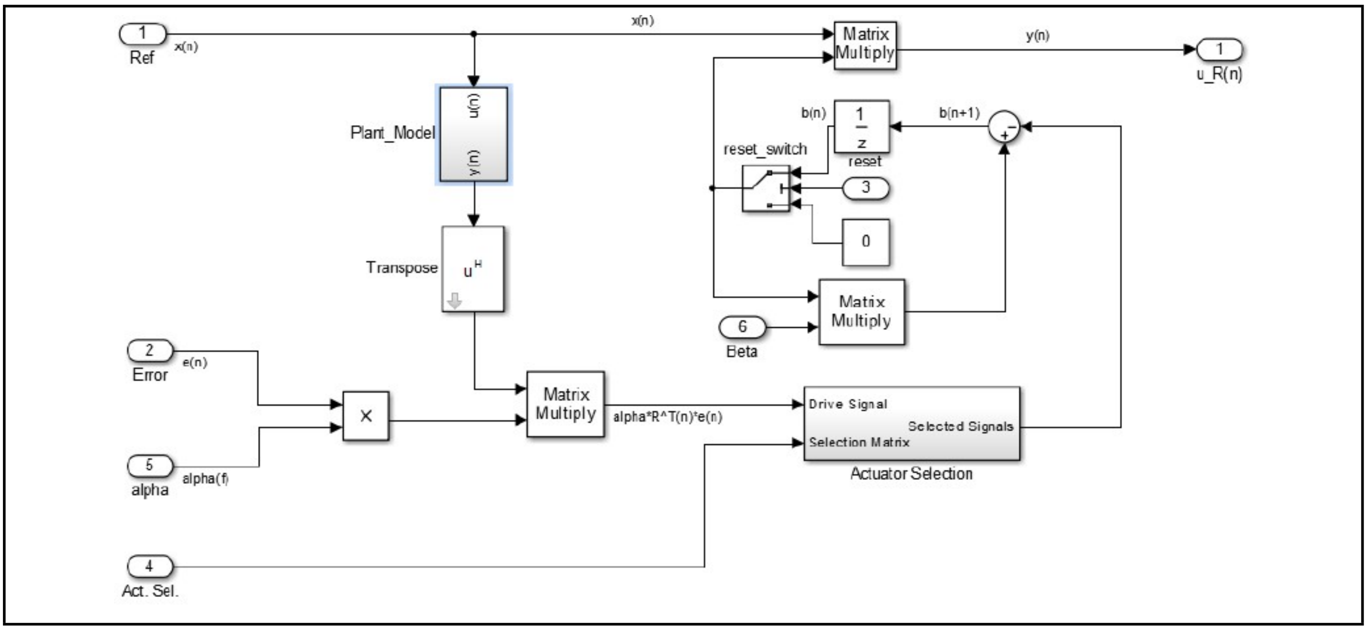

Figure 21. Schematic of FxLMS controller (“LMS_Quadrature” block).

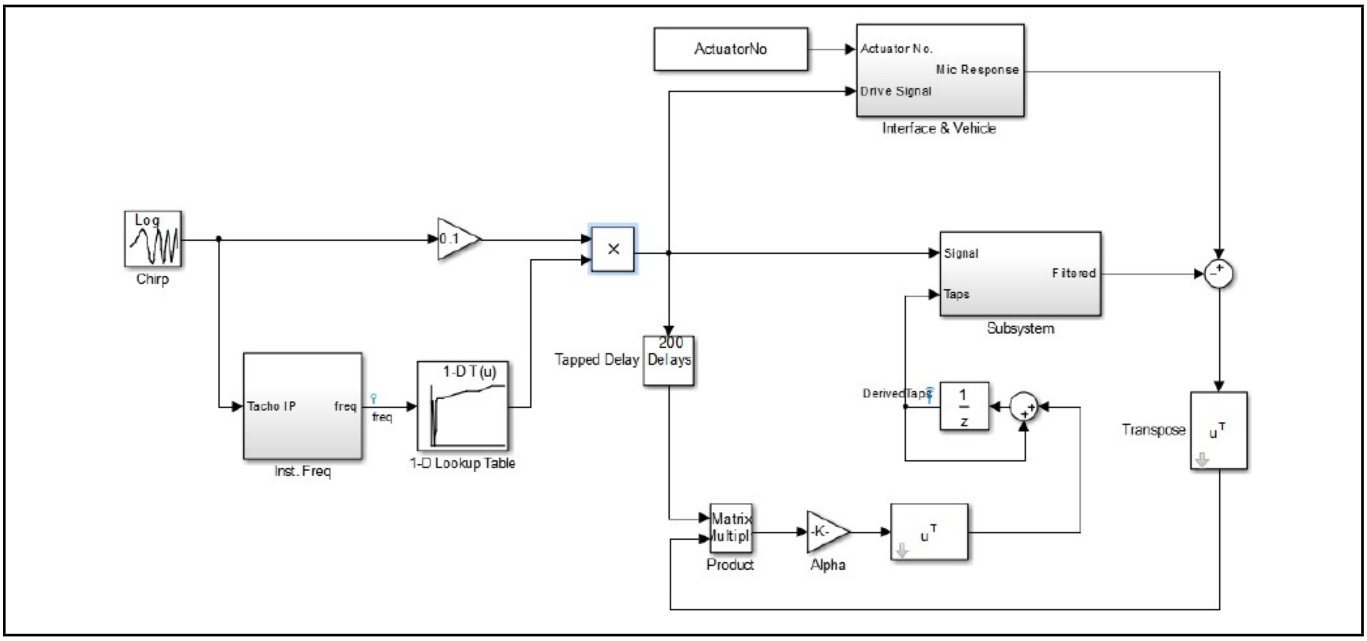

Figure 22. Schematic of system identification process.

5. CONCLUSIONS

A methodology of active noise control using vibration actuators has been developed to reduce engine noise inside the vehicle. The system was configured to implement the FxLMS algorithm with electromagnetic vibration generators mounted on the body member and acoustic error sensors mounted in the cabin. In this study, the appropriate number of error sensors and actuator positions have been decided through static noise reduction simulation, and the specifications of actuators have been proposed by estimating the magnitude of the force required for active noise control. From this result, four microphones on the left and right sides of each of the front and rear seats have been used as error sensors, and two electromagnetic inertial actuators with a force of up to 30 N have been installed in the front body side member close to the vehicle's engine mounts. For ANC logic, convergence coefficient has been entered as a frequency-dependent value to optimize convergence speed and stability together. In addition, the FxLMS algorithm supplemented by the beta scheduling method has been adopted to distribute power efficiently and prevent overrun issues that may occur because the actual available force of the actuator is less than the force required to reduce the vehicle noise. Through sensor and actuator selection, the introduced algorithm has been implemented in a four-cylinder diesel vehicle to reduce the second order engine noise level between 1800 and 3000 rpm. As a result of static tests and driving tests on a vehicle, it has been confirmed that the target noise component can be reduced by about 7 to 10 dB in the front and rear seats when using the proposed system. It has been also confirmed that there is a noise reduction effect at the center of the rear seat slightly away from the error sensors on the left side of the rear seat and the right side of the rear seat, which is expected to be due to the advantages of this method. In ad-

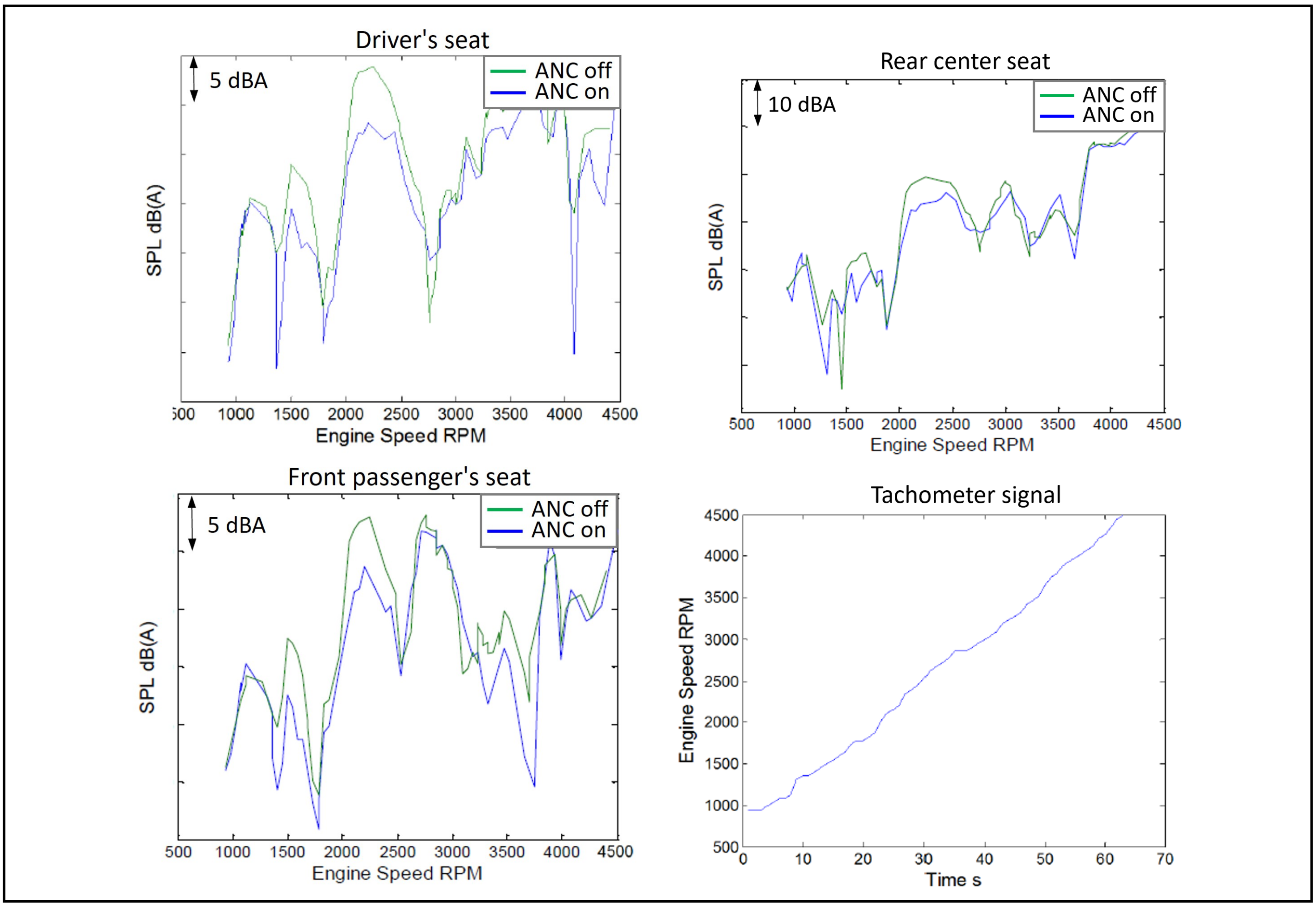

Figure 23. ANC test results on no-load run up.

dition, through noise reduction simulation, the case of exciting the body member around engine mounts as in this study and the case of exciting the body panel such as the cowl top panel as in the previous study have been compared. As a result, the latter has the advantage of being able to effectively control with less force, although it is difficult to control. On the other hand, the former has the advantage of having a greater noise reduction, although the required force is much greater. Through this study, it was expected that above two cases of the vibration-based ANC technology would be selectively available depending on the object to be controlled, the location of actuator attachment, and the limitations of weight. In terms of weight and performance, the ANC exciting around engine mounts was suitable for achieving higher noise reduction and vibration reduction together while allowing sufficient layout and heavy weight around the engine mounts. On the other hand, the ANC exciting body panels was suitable for obtaining an appropriate level of noise reduction while allowing only a small weight of actuators. In terms of noise type to be controlled, the ANC exciting around engine mounts was suitable for improving the noise transmitted through the structure with a clear noise source location, but it was not suitable when the noise source was widely distributed or the air borne sound was dominant, such as wind noise and road noise. As already described in the introduction, this ANC technology can also have high control stability as the primary path and the secondary path are almost identical when reducing the structure borne noise generated by the engine. However, since the driving environment of the vehicle is so diverse and complex, detailed measures such as applying different convergence coefficient for each condition or increasing the leaky factor can be used to clearly block the possibility of divergence. In addition, a reliability issue must be checked for mass production although it has not been confirmed in this study. It is particularly necessary to insulate vibration so that repeated shocks and vibrations from the road surface do not damage the actuator.

ACKNOWLEDGEMENT

This study has been conducted through the research project by the Institute of Sound and Vibration Research (ISVR) and Hyundai Motor Company. The authors are grateful to the ISVR members at the University of Southampton.

REFERENCES

1. Kajikawa, Y., Gan, W., and Kuo, S. Recent advances on active noise control: Open issues and innovative applications, *APSIPA Transactions on Signal and Information Processing*, **1**(1), E3, 1–21, (2012). https://doi.org/10.1017/ATSIP.2012.4

2. Cheer, J. Active Sound Control in the Automotive Interior, In: Fuchs, A. and Brandstätter, B. (Editors) *Future interior concepts*, Springer, 53–69, (2021). https://doi.org/10.1007/978-3-030-51044-2_3

3. Ferrari, C. L., Cheer, J., and Mautone, M. Investigation of an engine order noise cancellation system

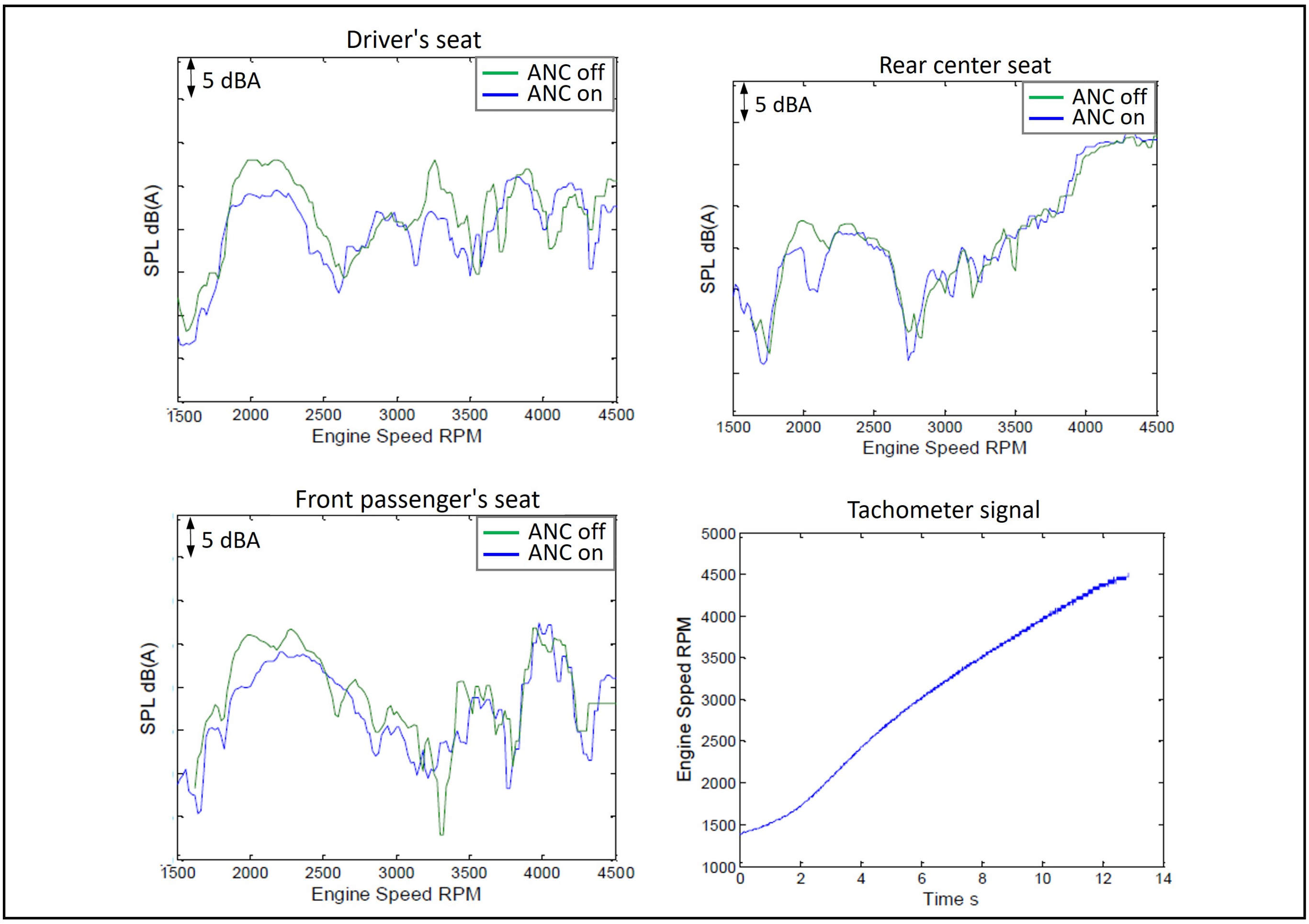

Figure 24. ANC test results on the 3rd gear WOT.

in a super sports car, *Acta Acustica*, **7**(1), (2023). https://doi.org/10.1051/aacus/2022060

4 Fuller, C. R. and Flotow, A. H. Active control of sound and vibration, *IEEE Control Systems Magazine*, **15**(6), 9—19, (1995). https://doi.org/10.1109/37.476383

5 Oliveira, L. P. R, Janssens, K., Gajdatsy, P., Auweraer, H. V., Varoto, P. S., and Desmet, W. Active sound quality control of engine induced cavity noise, *Mechanical Systems and Signal Processing*, **23**(2), 476–488, (2009). https://doi.org/10.1016/j.ymssp.2008.04.005

6 Shoureshi, R. A., Vance, J. L., Ogundipe, L., Schaaf, K., Eberhard, G., and Karkosch, H.-J. Active vibro-acoustic control in automotive vehicles, *SAE Transactions, J. of Passenger Cars: Part 2*, **106**(6), 2591–95, (1997). https://doi.org/10.4271/971886

7 Buttelmann, M., Lohmann, B., Marienfeld, P., Svaricek, F., Vinogradski, M., and Nedeljkovic, N. Online identification of active absorbers in automotive vibration control, *IFAC Proceedings Volumes: Advances in Automotive Control*, **34**(1), 187–192, (2001). https://doi.org/10.1016/S1474-6670(17)34396-3

8 Kraus, R., Herold, S., Millitzer, J., and Jungblut, T. Development of active engine mounts based on piezo actuators, *ATZ Worldwide*, **116**, 46–51, (2014). https://doi.org/10.1007/s38311-014-0012-7

9 Chang, K. J., Park. D. C., and Lee, Y. S. Active noise control using a body-mounted vibration actuator to enhance the interior sound of vehicle, International Journal of Automotive Technology, **23** (2), 327–333, (2022). https://doi.org/10.1007/s12239-022-0030-1

10 Elliott, S., Stothers, I. and Nelson, P. A multiple error LMS algorithm and its application to the active control of sound and vibration, *IEEE Transactions on Acoustics, Speech, and Signal Processing*, **35**(10), 1423–1434, (1987). https://doi.org/10.1109/TASSP.1987.1165044

11 Elliott, S. and Nelson, P. Active noise control, *IEEE Signal Processing Magazine*, **10**, 12–35, (1993). https://doi.org/10.1109/79.248551

12 Elliott, S. J. *Signal Processing for Active Control*, Academic Press, London, (2001). https://doi.org/10.1016/b978-0-12-237085-4.x5000-5

13 Cheer, J. Active control of the acoustic environment in an automobile cabin, *PhD thesis*, University of Southampton, (2012).

14 Douglas, S. C. A family of normalized LMS algorithms, IEEE Signal Processing Letters, **1** (3), 49–51, (1994). https://doi.org/10.1109/97.295321

15 Aboulnasr, T. and Mayyas, K. A robust variable step size LMS-type algorithm: analysis and simulations, *IEEE transactions on Signal Processing.* **45**(3), 63–639, (1997). https://doi.org/10.1109/78.558478